Pergamon

PII: S0021-8502(99)00544-3

www.elsevier.com/locate/jaerosci

J. Aerosol Sci. Vol. 31, No. 5, pp. 583–594, 2000

Printed in Great Britain
0021-8502/00/$ - see front matter

EXPERIMENTAL AND NUMERICAL STUDIES OF MICROSPHERE OBLIQUE IMPACT WITH PLANAR SURFACES

X. Li, P. F. Dunn* and R. M. Brach

Particle Dynamics Laboratory, Department of Aerospace and Mechanical Engineering, University of Notre Dame, Notre Dame, IN 46556, USA

(*First received* 25 *June* 1999; *and in final form* 17 *August* 1999)

Abstract—Oblique impact experiments have been carried out with stainless-steel microspheres and silicon surfaces under a range of impact velocities from 0.45 to 1.90 m s^{-1} and different incident angles. When the normal velocity component for oblique impact is less than the capture velocity as seen for normal impact, no capture was observed. The experimental results also reveal that the pattern of impulse ratio variation with incident angle varies with different initial impact velocities. Furthermore, the measured coefficient of restitution values can be predicted by a dynamic simulation model, and the measured impulse ratios can be matched if the microspheres are assumed to have initial angular velocities. © 2000 Elsevier Science Ltd. All rights reserved

1. INTRODUCTION

The oblique impact of a microsphere against a planar substrate surface in the presence of adhesion results either in capture by or rebound from the surface. There are a number of variables that can affect this process, such as the initial impact velocity, the incident angle with the substrate surface, the particle's size, its initial angular velocity, the substrate surface geometry, and the material properties of both the particle and the substrate.

Broom (1979) used the impact of glass spheres onto aluminum substrate to study the adhesion of particles in filters. The nominal impact angles were 90° and 45°. The results showed that the capture velocity was smaller for oblique impact. It was also found that the nature of the substrate surface was important; a polished surface exhibited an efficiency of capture higher than a rough surface.

Paw U (1983) studied the rebound of particles from natural surfaces. The experimental results revealed that for each type of particle, the capture velocity was almost the same irrespective of the surface materials. Size effects on the impact response were not studied in his experiments. In the analysis, he assumed that only the normal incident velocity component contributed to the rebound.

Aylor and Ferrandino (1985) conducted experiments with ragweed pollen and *Lycopodium* spore impact onto a cylinder. Their observations demonstrated that both the normal and tangential incident velocity components would determine the impact response. Further, the coefficient of restitution, e, defined as the ratio of rebound total velocity divided by the incoming total velocity, was not constant for impacts at different locations on the cylinder.

Wang and John (1988) investigated the adhesion efficiency of particles on a cylinder. Measurements of particle rebound as a function of the position angle on the cylinder showed that rebound increased rapidly with incident angle away from normal (90°). They suggested that the tangential velocity component caused particle bounce.

Buttle *et al.* (1989) conducted experiments with the impact of glass spheres onto aluminum substrates at normal, 50° and 29°. The value of coefficient of restitution increased from around 0.50 at the normal and 50° cases to 0.68 at the 29° case. This observation was

* Author to whom correspondence should be addressed.

considered to be the result of a reduction in the frictional force and of rotation of the particle for very oblique impacts.

The effects of incident angle, the microsphere's initial angular velocity and substrate surface roughness have been studied by Dunn *et al.* (1996). They found for molecularly smooth surfaces that the coefficient of restitution decreased by decreasing the initial velocity's normal component. The impulse ratio changed noticeably with incident angles. Their numerical studies showed that the initial angular velocity of microsphere was very important in determining the particle's rebound response. The initial impact velocity in their experiments was approximately 1.80 m s^{-1}, and no capture was observed. In Li *et al.* (1999), both experimental and numerical studies were carried out to investigate the effects of impact velocity and particle size on normal incidence impact response (90°). For the same type of microsphere and substrate surface used by Dunn *et al.* (1996), the results showed that capture occurred at an impact velocity of approximately 0.20 to 0.30 m s^{-1}, and for the same materials, the larger the particle size, the smaller the capture velocity.

In the present paper, oblique impact experiments have been carried out to investigate the effects of initial impact velocity and incident angle. The average initial impact velocity for eleven cases varied from 0.45 to 1.90 m s^{-1}. For each velocity case, the incident angle varied from 10 to 85° to examine incident angle effect on impact response. The main purpose was to determine whether or not restitution, $e(v_n)$, was the same for normal impacts as for oblique impacts.

Variations of the impulse ratio, μ, with incident angle at the same impact velocity have been studied systematically for the first time. The impulse ratio is interpreted as a friction coefficient when microsphere is sliding throughout the entire contact duration. The measured impulse ratio results of Dunn *et al.* (1996) support this hypothesis. Whether the previous observation is true for different initial impact velocities is examined here. The measured results of the translational kinetic energy loss, TK_L, are understood better in the light of the rigid-body impact mechanics developed by Brach and Dunn (1995). Finally, the numerical simulations are compared with the experimental results.

2. EXPERIMENTAL SYSTEM AND APPROACH

The basic experimental facility used for these experiments was developed by Caylor (1993) and described by Dunn *et al.* (1995). The system primarily consisted of a vacuum test cell (maintained at 10^{-5} kPa), a particle dispenser and a target surface. In these experiments, the microparticles were dispensed using a neutral-charge particle dispenser (NPD). The microparticles were placed on the bottom dispenser plate of the NPD. A rotor underneath the plate periodically contacted the plate and vibrated it, causing the microspheres to fall through a hole at its center. To control the falling particles, a hypodermic needle was connected to the hole. As a result, the microspheres were directed downward in a straight trajectory to the target surface. Once a particle was ejected from the NPD, it was accelerated by gravity to the target surface. The vertical distance between the dispenser and the target surface varied from 0.01 to 0.2 m, providing a velocity range from 0.44 to 2.0 m s^{-1}.

For oblique impact experiments in which the target surface was inclined at an angle with respect to the incident particle beam, a particle trajectory imaging system (PTIS) was used to record the microparticles incident and rebound trajectories, from which the velocity components were determined. This setup is shown in Fig. 1. The PTIS was comprised of an Argon ion laser, beam chopper, plano-convex lens, CCD camera and video recorder. The PTIS generated a pulsed laser light sheet that illuminated the individual particle as it approached and rebounded from the surface. The trajectory images were processed to obtain the particle's incident and rebound angles and speeds. For this PTIS setup, an argon ion laser beam (operated nominally at 2 W) passed through a collimator to control the beam width to provide a narrow light sheet as possible. The laser beam was then directed through a spinning disk with 10 evenly spaced slots to produce a pulsed laser beam. Depending on the angular velocity of the disk, the pulsed frequency could be varied to

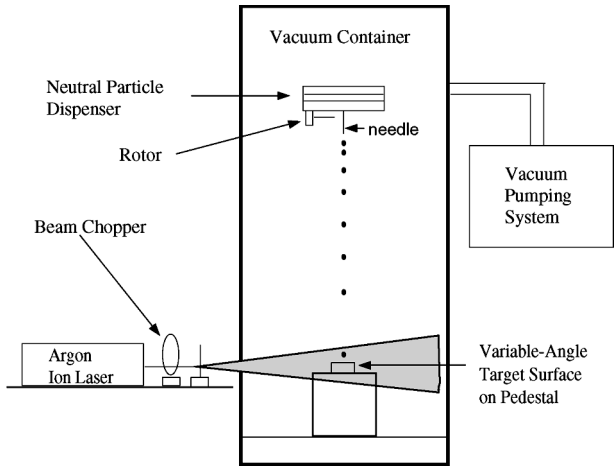

Fig. 1. Schematic of the experimental system: side view.

obtain the desired track length. The chopped beam went through a plano-convex lens that formed a pulse light sheet aligned in a vertical plane above the target surface and in the plane of particle trajectory. In preparing an experiment, another laser beam was sent through the hypodermic needle to make sure this laser beam was at the center of the pulsed light sheet. Video data were taken through an optical viewport located at the side of the vacuum chamber using a CCD camera and a video cassette recorder. The camera was placed approximately 90° to the light sheet. Based on the camera's frame rate, the field of view, and the strobe frequency, the system could measure particle velocities ranging from ~ 0.1 to 30 m s^{-1}.

The configuration and coordinate system for processing the experimental data is illustrated in Fig. 2. The velocity components for the normal and tangential directions are calculated from the angles of incidence and rebound. Based on the rigid-body model of Brach and Dunn (1995), these velocity components are used to determine three parameters that characterize the impact event. These are the coefficient of restitution, e, the impulse ratio, μ, and the normalized kinetic energy loss, TK_L. They are defined as

$$e = -\frac{V_n}{v_n}, \tag{1}$$

$$\mu = \frac{P_t}{P_n} = \frac{V_t - v_t}{V_n - v_n}, \tag{2}$$

$$TK_L = \frac{v^2 - V^2}{v^2} = [1 - e^2 + 2\mu(1+e)\eta - \mu^2(1+e)^2]/(1+\eta^2), \tag{3}$$

where the subscript n denotes the normal direction, and t the tangential direction; the symbol V means the rebound velocity and the symbol v the incoming velocity; P_t and P_n are the impulse in the tangential and normal directions during the entire contact duration, respectively; $\eta = (v_t - r\omega)/v_n$, where r is the non-deformed particle radius and ω the particle's initial angular velocity. If $\omega = 0$, then, $\eta = \tan^{-1}\alpha_i$.

In the following experiments, only one type of substrate surface and one type of microsphere were used. The target surfaces were specially prepared from a [1,0,0] plane silicon crystal wafer. An atomic force microscope scan of the surface verified that the surface was molecularly smooth (the surface asperity height standard deviation was approximately 10 Å). After the impact experiment at each incident angle for a velocity level, the substrate surface was changed to avoid any ambiguities in surface quality.

The microspheres were commercially available type 316 stainless steel with a nominal diameter range of 64–76 μm. Their surfaces appeared visually smooth to within the

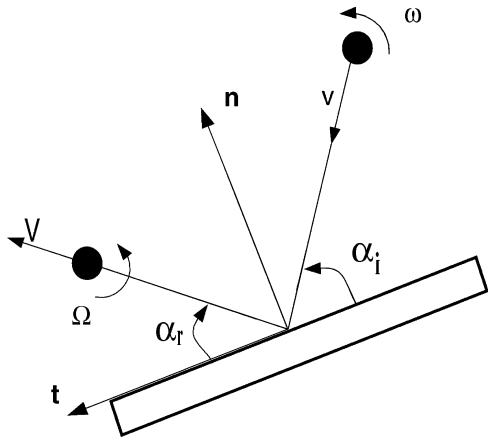

Fig. 2. Definition of velocity components and incident angles.

resolution of the scanning electron microscope used to view a sample of the microspheres. The dispenser height was varied from 20 to 0.8 cm to obtain impact velocities ranging from 2.00 down to 0.40 m s^{-1}. At each height, the target surface was rotated to achieve a range of different incident angles. For fixed conditions, the largest variation in initial velocity from the nominal value was $\pm 13\%$ (the largest variation was for the lowest initial velocity).

The uncertainties of the velocity and angle arise from the variations in measuring distance and angles as recorded on the video images, and from the variations of strobe frequency. These variations change with the incident angle and combine to yield uncertainties in velocity components and incoming and rebounding angles. By using a standard uncertainty analysis, uncertainties for final results e, μ and TK_L can be estimated with 95% confidence. Consequently, in the following presentation, the sample mean value of an experimental quantity is plotted with an error bar denoting 95% confidence ($\pm$ two sample standard deviations). The sample mean value of each quantity is determined by first computing the quantity's value for each individual impact event and then ensemble averaging the values of all the events detected (about 40 events for each plotted data point).

3. EXPERIMENTAL RESULTS

3.1. *Coefficient of restitution*

Figure 3 shows the coefficient of restitution plotted as a function of incident angle. Figure 4 shows the coefficient of restitution from the same data plotted as a function of the initial normal velocity component. Both are for the nominally constant total incident velocities of 1.60 m s^{-1} (1.59 m $s^{-1} < v_i <$ 1.69 m s^{-1}), 1.05 m s^{-1} (1.01 m $s^{-1} < v_i <$ 1.09 m s^{-1}) and 0.45 m s^{-1} (0.39 m $s^{-1} < v_i <$ 0.49 m s^{-1}). For the low initial impact velocity case ($v_i = 0.45$ m s^{-1}), the trend of decreasing coefficient of restitution with decreasing incident angle is the most noticeable. The values of the coefficient of restitution decrease from about 0.80–0.60 as the angle of incidence changes from 85 to 30°. But for the highest initial impact velocity case, $v_i = 1.60$ m s^{-1}, the decrease in the coefficient of restitution is slight and the trend is not consistent at very shallow incident angles. As shown in the plot, the average value changed from 0.70 to 0.65 with the incident angle decreasing from 85 to 25° for $v_i = 1.60$ m s^{-1} case.

Figure 4 shows that the coefficient of restitution changes with the decreasing of normal velocity component. As the incident angle decreases, the normal velocity component also decreases, creating a condition where adhesion reduces the restitution. For some cases shown in Fig. 4, the normal velocity components are lower than the capture velocities measured in previous experiments for normal impact (0.2–0.3 m s^{-1} for the diameter range of 64–76 μm in Li *et al.*, 1999). Yet, no capture is observed and the coefficient of restitution is

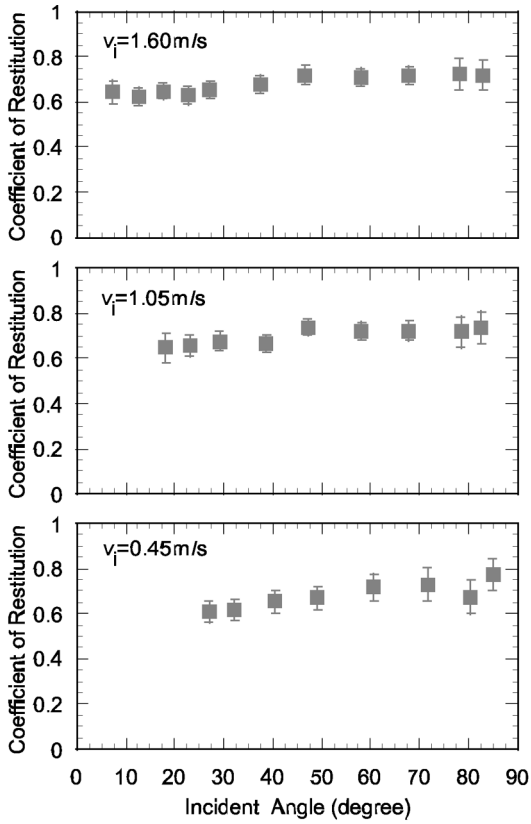

Fig. 3. The coefficient of restitution vs. incident angle.

still rather high. This implies that for oblique impact, the capture velocity is different from and lower than that for normal impact.

This finding is interesting because the current understanding of adhesion and friction and their modeling using impact mechanics indicate that adhesion and friction are uncoupled. This means that the presence of an initial tangential velocity should not affect the normal process of impact. The data of Fig. 4 imply otherwise. These results further demonstrate that the process of capture of microparticles is more complex than presently thought and that capture is more likely for normal impacts than for oblique impacts.

3.2. *Impulse ratio*

For the same experimental collisions described above, the change of impulse ratio with the incident angle is shown in Fig. 5. For $v_i = 1.60\ \mathrm{m\ s^{-1}}$, in the region of incident angles from 85 to 50°, the impulse ratio increases with the decreasing incident angle. This region is the "rolling region", where the microspheres are rolling on the surface at the end of contact. Starting from about 50 down to 10°, the impulse ratio changes little, is approximately constant and equal to about 0.15. This is the "sliding region", where the microspheres are sliding on the surface throughout contact. A constant impulse ratio can be interpreted as a coefficient of friction that obeys Amontons–Coulomb's law as illustrated by the solid line in Fig. 5, from the rigid-body impact model. The comparison shows that the application of rigid-body impact mechanics to this case is very successful. For the cases of $v_i = 1.05$ and $v_i = 0.45\ \mathrm{m\ s^{-1}}$, the impulse ratio still increases when the incident angle decreases from 85°, but the increasing region becomes narrower. After that, the impulse ratio is not constant; it decreases with decreasing incident angle. Some values even are less than or close to zero, which implies a negative or zero frictional impulse. The reason for the decrease of the

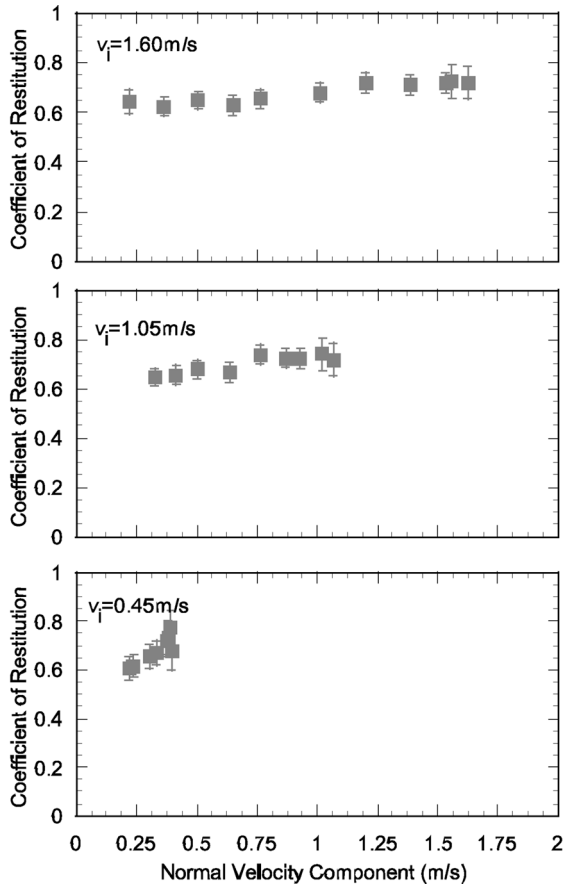

Fig. 4. The coefficient of restitution vs. initial normal velocity component.

impulse ratio with decreasing incident angles is not clear. There are two hypotheses proposed to explain this observation.

The first hypothesis is that the anomalous behavior possibly is due to unknown and/or uncontrolled variations in the initial angular velocity, ω. The true impulse ratio for the "sliding region" should be the same as that found in the case with initial impact velocity $v_i = 1.60\,\mathrm{m\,s^{-1}}$, which was 0.15 for this contact system. An initial angular velocity affects the contact mode, giving either rolling or sliding on the surface. Thus, the angular velocity influences the sliding duration. As a result, the impulse ratio is affected. This hypothesis will be applied and clarified in Section 4.

Brach (1991) also pointed out that the presence of relatively large forces and a short contact duration during impact add more complexity to the generation of the frictional force. Consequently, the interpretation of the impulse ratio, μ, and whether or not μ represents the Coulomb friction coefficient, f, should be treated with care. Generally speaking, if a Coulomb friction model is appropriate for impact, then, the experimental results of the impulse ratio should follow a trend as shown in the top plot of Fig. 5. Other trends as shown in the middle and the bottom plots of the same figure can imply a tangential process governed by other than a simple friction law.

The second hypothesis assumes that Coulomb's law applies but that the friction coefficient can vary significantly as a function of the initial tangential velocity. For example, for the $v_i = 1.05\,\mathrm{m\,s^{-1}}$ case, the tangential velocity variation from 0.20 to $1.00\,\mathrm{m\,s^{-1}}$ would account for the observed change in the impulse ratio. However, such high dependence of f on tangential velocity has not been observed before.

Tabor (1981) thoroughly reviewed the studies related to friction. He pointed out three areas that need more understanding: true contact area, interfacial bonds and deformation

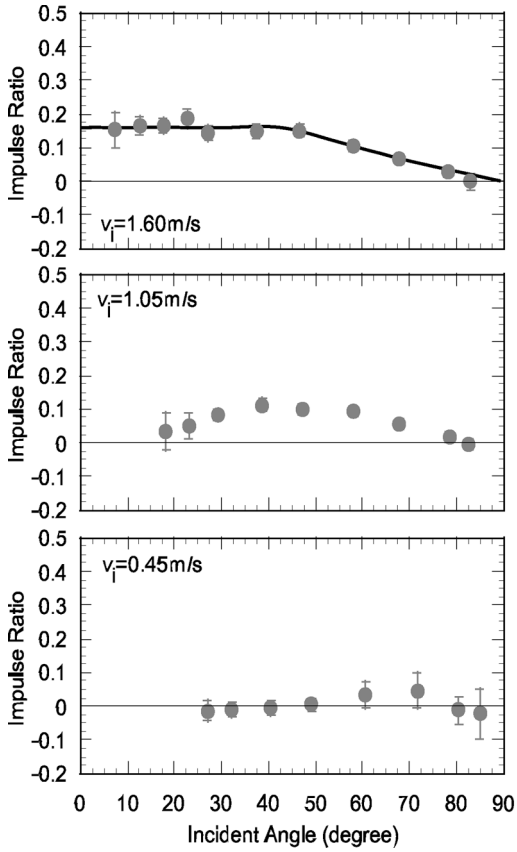

Fig. 5. The impulse ratio vs. incident angle (solid curve is from rigid-body impact mechanics).

processes during sliding. Generally speaking, the friction force can be a function of the normal pressure, relative sliding velocity, temperature, contact time and other unspecified external factors between the contact surfaces. These factors can also be categorized into: (1) surface geometrical structure, (2) the nature of surface forces, and (3) material properties of the surface itself. Even with the advanced instruments, such as atomic force microscope (AFM) and the friction force microscope (FFM), many questions about the friction force still have to be answered Krim (1996), particularly for microparticle contact and especially for impact.

3.3. *Normalized energy loss*

The rotational energy loss cannot be measured in the present experimental setup. So, only the translational kinetic energy loss is reflected in experimental measurements. The variations of the translational kinetic energy loss, TK_{L}, are plotted with the incident angle in Fig. 6 (same data as shown in Figs. 3 and 5). For the highest nominal initial velocity, $v_i = 1.60\,\mathrm{m\,s^{-1}}$, TK_{L} is approximately constant from 85 down to 50°. From equation (3), when the incident angle is large and μ is small, $TK_{\mathrm{L}} \sim (1 - e^2)$. Because values of the coefficient of restitution change very slightly (see Fig. 3) for this region, as a result, there should be no differences in TK_{L}. With the incident angles decreasing from 50°, the normalized energy loss decreases consistently to near zero. Based on rigid-body mechanics, under an irrotational initial condition, when the incident angle decreases, η^2 increases faster than η, and both are larger than unity for $\alpha_i < 45°$. Therefore, as seen from equation (3), TK_{L} almost always decreases with decreasing small incident angles.

At $v_i = 1.05\,\mathrm{m\,s^{-1}}$, the range of constant normalized energy loss region becomes narrower (60–85°). This is even more obvious for $v_i = 0.45\,\mathrm{m\,s^{-1}}$ case, where the normalized

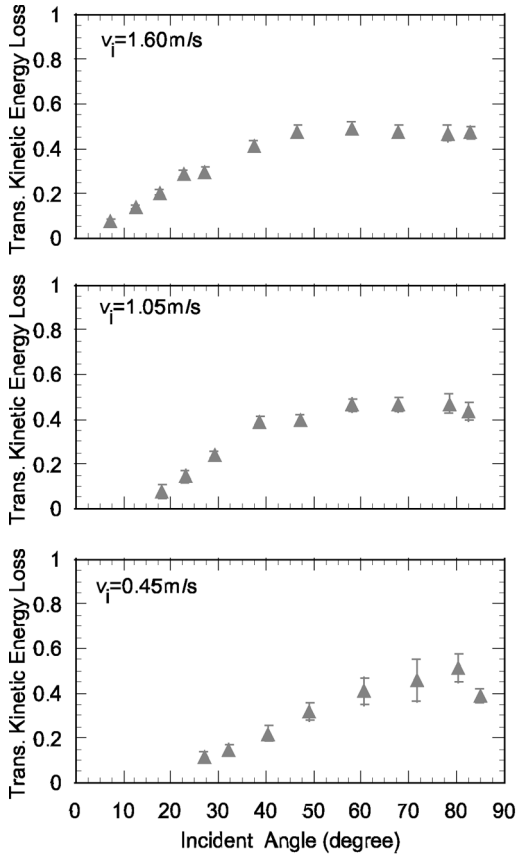

Fig. 6. The normalized energy loss vs. incident angles at three different initial impact velocity levels.

energy loss decreases steadily starting from 80°. If capture correlates with energy loss, it is clear that capture is more likely for normal impacts.

4. NUMERICAL SIMULATIONS

There are very few models proposed to simulate oblique impact. In the numerical simulation model for microspheres developed by Brach and Dunn (1995), the governing equations of motion in the normal, tangential directions and the rotational motion are as follows:

$$m\ddot{n} = -\sqrt{r}Kn^{3/2}(1 + C_{\mathrm{H}}\dot{n}) + 2\pi a f_0(1 + C_{\mathrm{A}}\dot{n}), \tag{4}$$

$$m\ddot{t} = F_{\mathrm{t}}(\tau) = \begin{cases} -f[-\sqrt{r}Kn^{3/2}(1 + C_{\mathrm{H}}\dot{n}) + 2\pi a f_0(1 + C_{\mathrm{A}}\dot{n})] & \text{if } \dot{t} - r\dot{\theta} \neq 0, \\ 0 & \text{if } \dot{t} - r\dot{\theta} = 0, \end{cases} \tag{5}$$

$$mK^2\ddot{\theta} = -rF_{\mathrm{t}}(\tau), \tag{6}$$

where n is the mass center displacement in the normal direction, t displacement in the tangential direction; C_{H} and C_{A} are damping constants; $\dot{\theta} = \omega$, the angular velocity; K, the radius of gyration of a sphere, and r, the sphere radius. K is the equivalent Hertzian stiffness and defined as

$$K = \frac{4}{3\pi(k_1 + k_2)}, \tag{7}$$

$$k_i = \frac{(1 - v_i^2)}{\pi E_i}, \tag{8}$$

where E and v are Young's modulus and Poisson ratio for a given material, respectively. In equation (4), the first term of the right-hand side is the Hertzian contact force and its dissipation, while the second term is the adhesion force and its dissipation. The adhesion force is modeled as a ring force, $2\pi a f_0$, where a is contact radius as determined from Hertzian theory as a function of time, τ, where $a^2(\tau) = rn(\tau)$. f_0 is the adhesion force per unit length, and is determined from $f_0 = (18\, Kr\gamma_1\gamma_2/\pi)^{1/3}$, where γ_i represents the traditional free surface adhesion energy of each material. Procedures to determine f_0 are given by Li *et al.* (1999). Amontons–Coulomb's law is applied in the model to determine the friction force. Etsion and Amit (1993) experimentally studied the effects of small normal loads on the static friction coefficient for smooth surfaces. They found a dramatic increase in the static coefficient of friction when the normal load was reduced. They conjectured that this was caused by the adhesion force. In this simulation, the adhesion force and its dissipation contribute to the friction force by their influence on the normal force.

The energy loss is modeled by the dissipation terms in equation (4) with damping coefficients C_H and C_A. Although energy loss is attributed to plastic deformation in some papers, such as Xu and Willeke (1993), there is no experimental evidence to support that plastic deformation occurs for the low-velocity impact of microspheres. The exceptionally high strain rates and size effects for microparticle impacts make the likelihood of plastic deformation minimal. Moreover, at low velocities, the dissipation due to adhesion is much more significant than material dissipation (see Brach and Dunn, 1995). In the present model, the energy loss is treated as hysteresis. C_H is non-dimensionalized by the Hertzian contact duration time, T, and the non-deformed microparticle radius r, where $\zeta_H = rC_H/T$. Likewise, the damping coefficient C_A is treated as ζ_A in the simulation. ζ_H and ζ_A are determined by matching the simulations of the coefficient of restitution to the experimental values at highest incident angle $\alpha = 85^\circ$ and the lowest incident angle by an iteration scheme. In the following, this simulation approach was applied to model oblique impact at different initial impact velocities, where the results are compared with the experimental measurements. For the present simulations, the following values were used: $r = 35\ \mu$m, $f_0 = 314\ \mathrm{N\,m^{-1}}$, and $K = 111.4$ GPa. For the case of $v_i = 1.60\ \mathrm{m\,s^{-1}}$, $\zeta_H = 25$ and $\zeta_A = 1100$ were chosen using the aforementioned iteration scheme.

In Fig. 7, the solid symbols represent the same experimental results shown in Fig. 3, and the solid lines are from the numerical simulation. It is seen that the trend of the coefficient of restitution is well simulated generally by choosing appropriate Hertzian and adhesion dissipation coefficients, ζ_H and ζ_A. The simulation predicts a more significant decrease of the coefficient of restitution at smaller incident angles than experimental observations for the $v_i = 1.60\ \mathrm{ms^{-1}}$ case. For the lower velocity cases, the simulation matches the experimental values well. For oblique impact, the adhesion force may be reduced by the existence of friction (Toikka *et al.*, 1999). Such a relation between adhesion and friction is not fully understood yet and therefore not modeled in the simulation.

In the subject simulations, Coulomb's coefficient of friction, f, was chosen as 0.15 based upon the experimental data for the initial impact velocities greater than $1.50\ \mathrm{m\,s^{-1}}$. For these cases, within a certain range of shallow angles, the impulse ratio was approximately a constant value of 0.15. The simulations of the impulse ratio were carried out for the three different initial impact velocities. The results for the case of $v_i = 0.45\ \mathrm{m\,s^{-1}}$ are plotted as the solid curves along with the measured values for the upper plot in Fig. 8. This comparison shows that the simulations do not agree with the experimental results for the lowest initial velocities. This is probably the result of the microspheres having an initial angular velocity, which was not measured and modeled.

To see if initial angular velocity can cause low impulse ratio values and match the experimental results, an inverse approach was used. The initial angular velocity was varied in the simulation until a match was achieved with the measured impulse ratio, as shown in the lower plot of Fig. 8. The initial angular velocities are different for different incident angles. The same process of matching μ was done for the other two velocities. The initial angular velocities are also different for each impact velocity, but the pattern is the same (see Fig. 9). The angular velocity is plotted in Fig. 9 as the product of $r\omega$. For the higher incident

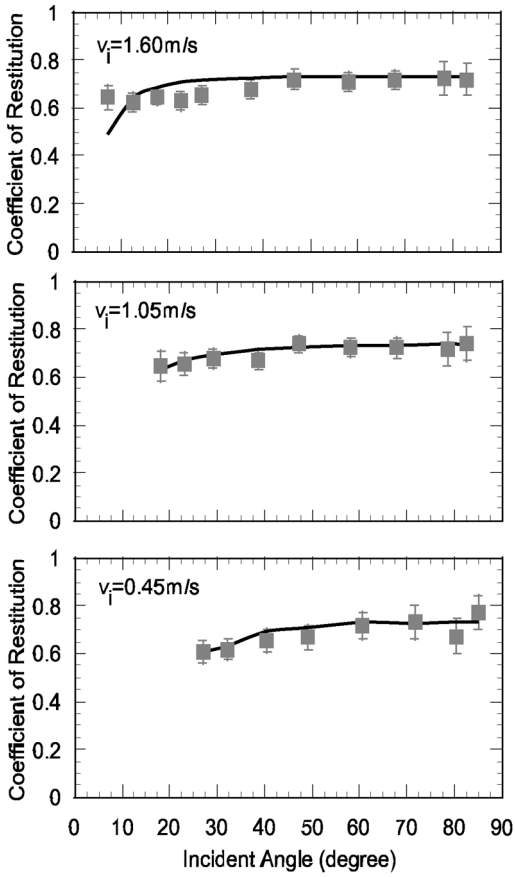

Fig. 7. Numerical simulation for the coefficient of restitution at three initial impact velocity levels.

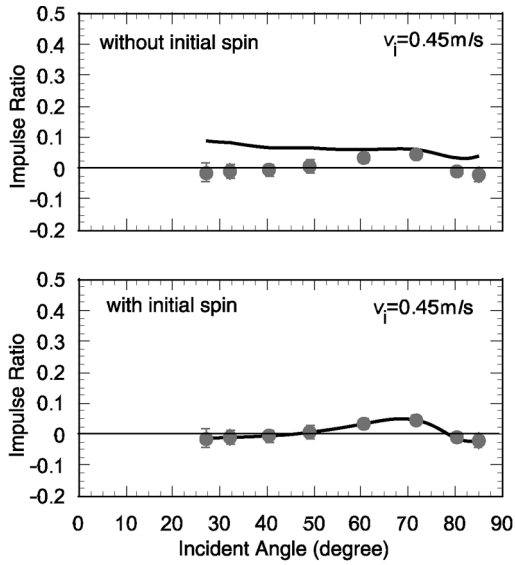

Fig. 8. The numerical simulation for the impulse ratio without/with initial angular velocity.

angles, the required initial angular velocity is small and near zero. For the shallower angle impact, the required angular velocity becomes larger. The magnitude of $r\omega$ is always less than the initial tangential velocity. $r\omega$ values on the order of 1.00 m s^{-1} are possible with the present experimental setup. The microspheres can roll along inside of the dispenser's exit

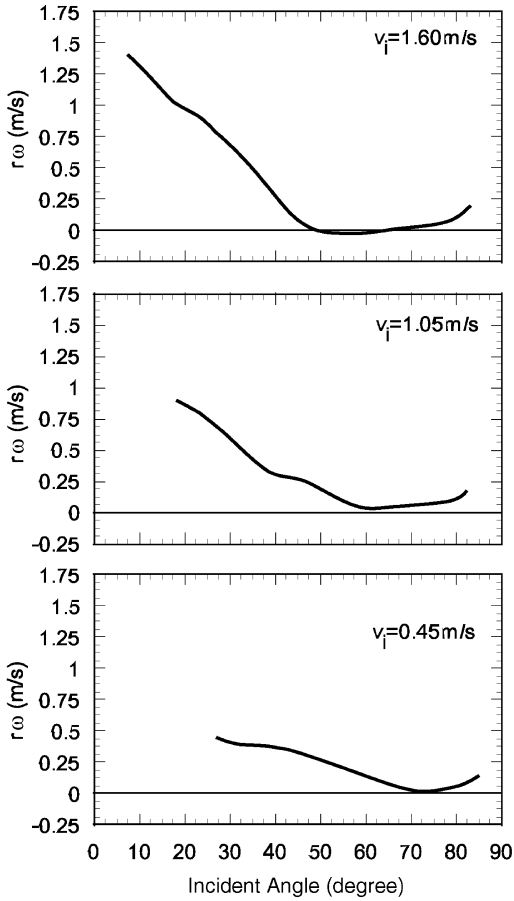

Fig. 9. The initial $r\omega$ vs. the incident angle at different initial impact velocities.

needle before ejection, thereby gaining rotational velocity in the process. However, the dependence of $r\omega$ upon the incident angle presently cannot be explained.

The numerical simulation was used at the incident angle of $\alpha = 50^\circ$ for two different initial velocities, $v_i = 1.05$ and $v_i = 0.45\,\mathrm{m\,s^{-1}}$, to match the impulse ratios with the experimental values. The adhesion force per unit length, f_0, and the two dissipation coefficients, ζ_H and ζ_A, were the same in those computations. The results show that for both cases, sliding ended and the microsphere was rolling at separation. The sliding duration was longer for the larger initial velocity at the same incident angle, which generated a higher value of the impulse ratio. According to the simulations, in order to match the experimental impulse ratio values, the particles first had sliding motion and then, finally changed to no sliding before the end of contact. If the incoming particle had a high tangential velocity component, the required rotational speed to achieve rolling without sliding before leaving the surface also was quite high. That is why the rotational speed increased with decreasing incident angles from 50° to very shallow angles, as is shown in Fig. 9.

5. CONCLUSIONS

The present experiments have systematically studied the oblique impact of microspheres under a range of impact velocities from 0.45 to $1.90\,\mathrm{m\,s^{-1}}$. They have provided new information about microsphere impact with an inclined substrate surface.

It was found that when the normal velocity component for oblique impact is less than the capture velocity observed for the normal impact, no capture is observed. This supports that the capture velocity for oblique impact is different from that for normal impact. The

experimental results also reveal that the pattern of impulse ratio variation with incident angle depends on the initial impact velocity.

The numerical simulation showed that the variation of impulse ratio can be explained by including the effect of the particle's initial angular velocity. Whether or not the observed impulse ratio variation was due directly to initial angular velocities is not clear because direct measurement of the microsphere's rotational velocity is not possible with the present setup. Furthermore, the numerical simulations have supported that coefficient of restitution can be simulated reasonably well by the present model. Finally, for the same incident angle, a longer sliding contact duration will yield a higher impulse ratio value.

Acknowledgements—The research described in this article was supported in part by the Center for Indoor Air Research (Contract No. 96-06) and in part by the Electric Power Research Institute (Contract No. RP 8034-03).

REFERENCES

Aylor, D. E. and Ferrandino, F. J. (1985) *Atmos. Environ.* **19,** 803–806.
Brach, R. M. (1991) Mechanical Impact Dynamics. New York: Wiley.
Brach, R. M. and Dunn, P. F. (1995) *Aerosol Sci. Technol.* **23,** 51–71.
Broom, G. P. (1979) *Filtration Separation* **16,** 661–669.
Buttle, D. J., Martin, S. R. and Scruby, C. B. (1989) Harwell Laboratory Report AERE-R13711: Oxfordshire, UK, pp. 1–30.
Caylor, M. J. (1993) The Impact of Electrically Charged Microspheres with Planar Surfaces under Vacuum Conditions. Ph.D. dissertation. University of Notre Dame.
Dunn, P. F., Brach, R. M. and Janson, G. G. (1996) *Aerosol Sci. Technol.* **25,** 445–465.
Etsion, I. and Amit, M. (1993) *J. Tribol.* **115,** 406–410.
Krim, J. (1996) *Sci. Amer.* 74–80.
Li, X., Dunn, P. F. and Brach, R. M. (1999) *J. Aerosol Sci.* **30**(4)**,** 439–449.
Paw, U. K. T. (1983) *J. Colloid Interface Sci.* **93,** 442–452.
Tabor, D. (1981) *J. Lubricat. Technol.* **103,** 169–179.
Toikka, G., Spinks, G. M. and Brown, H. R. (1999) Proc. 22nd Ann. Meeting of the Adhesion Society, pp. 14–16.
Wang, H. C. and John, W. (1988) In *Particles on Surface*, 1: *Detection, Adhesion, and Removal* (Edited by Mittal, K. L.), pp. 211–224.
Xu, M. D. and Willeke, K. (1993) *J. Aerosol Sci.* **24**(1)**,** 119–130.